JOURNAL OF GEOPHYSICAL RESEARCH, VOL. 105, NO. C6, PAGES 13,965–13,979, JUNE 15, 2000

A model study on internally generated variability in subtropical mode water formation

W. Hazeleger and S. S. Drijfhout

Royal Netherlands Meteorological Institute, De Bilt, The Netherlands

Abstract. Internally generated variability in the subtropical gyre is studied as a possible mechanism for the observed interannual to decadal variability in subtropical mode water formation. An isopycnic ocean model with idealized geometry and forcing which mimics the North Atlantic subtropical gyre is used for this purpose. The horizontal resolution is sufficiently high and the friction and diffusion sufficiently low for the flow to become barotropically and baroclinically unstable. Two modes of low-frequency variability are found. Both modes consist of westward propagating thickness anomalies. The anomalies have a first baroclinic modal structure with a maximum amplitude at the thermocline. One mode has a timescale of 8 years and a basin wide spatial scale; the other has a timescale of 4.5 years and a smaller spatial scale. The modes appear to be damped when the diffusion is high. In that case, the 8-year mode can be excited by a spatially coherent stochastic wind stress. The evolution of the modes is determined by an interaction between the mean flow and the low-frequency variability itself. The modes are instabilities of the mean flow determined by the basic stratification. It appears that coupling to the atmosphere and a parameterization of surface mixing are necessary for the low-frequency variability to appear in the mixed layer. The coupling and surface mixing do not play a role in generating the modes. It is concluded that these internally generated modes may play a role in the observed variability in mode water formation.

1. Introduction

In the subsurface layers of the subtropical gyre of the North Atlantic a distinct layer of constant density is found. This vertically homogeneous water mass covers almost the entire subtropical gyre west of the mid-Atlantic ridge. *Worthington* [1959] called this water mass 18°C water because of its nearly constant temperature of 18°C. Similar water masses are found in subtropical gyres of all ocean basins. These water masses were named "mode water" by *Masuzawa* [1969] because of their outstanding large volume of water with a uniform temperature and salinity, being a mode in the statistical sense.

Despite their stability, distinct interannual to decadal variability is observed in mode waters. This is displayed in one of the longest time series of oceanic data, including subsurface data, that has been collected at Panulirus station at Bermuda. At Panulirus a well-defined subsurface minimum in the vertical density gradient is found. This homogeneous layer corresponds to the mode water core. There are remarkable interannual to decadal changes in the properties of this mode water core (see *Talley and Raymer* [1982], updated by *Dickson et al.* [1996]). These variations have also been shown by *Joyce and Robbins* [1996] and *Jenkins* [1982]. *Molinari et al.* [1997] presented cross sections of temperature in the subtropical gyre for different periods. They showed that the changes in the Panulirus data reflect changes over the entire western subtropical gyre. Maximal changes of mode water thickness of the order of 50 m were found. Also, mode water characteristics in the North Pacific subtropical gyre show interannual to decadal changes [*Suga and Hanawa*, 1995]. Furthermore, slowly southwestward propagating subsurface anomalies are found in the Pacific, associated with variations in subduction [*Deser et al.*, 1996; *Zhang and Levitus*, 1997; *Tourre et al.* 1999].

Mode water is formed by subduction, mainly by a lateral induction through the large slope of the winter mixed layer depth [e.g., *Qiu and Huang*, 1995]. In winter, in the midlatitudes deep mixed layers are formed owing to large outgoing heat fluxes. Therefore the variability in mode water formation might be explained by variability in the surface heat flux in the formation area of mode water. However, both *Talley and Raymer* [1982] and *Jenkins* [1982] failed to find a good quantitative correlation between the variability in the surface heat flux and the variation in mode water properties in

Paper number 2000JC900041.
0148-0227/00/2000JC900041$09.00

the North Atlantic. Also, salinity changes at Panulirus were too large to be explained from local forcing alone [*Talley*, 1996]. This indicates that variability in mode water formation in the North Atlantic is not merely a result of variability in the surface forcing. On the other hand, qualitatively, the mode water variability correlates well with the North Atlantic Oscillation (NAO), as does the surface heat flux [*Cayan*, 1992; *Dickson et al.*, 1996]. Also, subtropical mode water in the southwestern North Pacific could not be explained by local atmospheric forcing alone [*Yasuda and Hanawa*, 1997]. *Suga and Hanawa* [1995] found only a good correlation between wintertime cooling and potential vorticity of the mode water core during the non-large-meander period of the Kuroshio. This motivates us to study other possible mechanisms of variability of mode water formation. We focus on mode water in the North Atlantic because its low-frequency variability is well documented by the Panulirus time series. However, the results may be applicable to low-frequency variability in any subtropical gyre.

By definition, externally generated oceanic variability is generated independently of oceanic processes, for instance, the passive response of the ocean to variability in the atmospheric forcing. As was stated above, the observations indicate that this cannot entirely explain the observed mode water variability. This has been confirmed in model studies [*Marsh and New*, 1996; *Hazeleger and Drijfhout*, 1998]. Another form of passive response of the ocean to the atmosphere is integration of high-frequency weather fluctuations to low-frequency variability in the ocean [*Hasselmann*, 1976]. The high-frequency forcing can excite oscillations that are damped otherwise [*Griffies and Tziperman*, 1995]. *Hazeleger and Drijfhout* [1999] have shown that such a mechanism can drive variability in mode water formation. Especially, stochastic heat flux forcing was found to generate variability in mode water formation of the observed magnitude, but no preferred timescale was found.

In the present study we will investigate whether internal variability, that is, complex interactions within the ocean itself, can explain the observed variability in mode water formation. A numerical model of an idealized subtropical gyre will be used for this purpose. The advantage of using a numerical model is that variations in the atmospheric forcing can be excluded. In this way, all variability in the model must be internally generated. Many model studies have been performed to study internal variability in the ocean associated with variability in the thermohaline circulation [e.g., *Weaver and Sarachik*, 1991]. Less attention has been paid to low-frequency internal variability of the subtropical gyre system associated with instabilities of the mean flow. Internal variability in the subtropical gyre may arise by horizontal and vertical shear or by nonlinear dynamics associated with the western boundary current, and midlatitude jets [e.g., *Jiang et al.*, 1995]. *Cox* [1987] was one of the first to demonstrate this type of variability in a primitive equation numerical ocean model. Here we will perform a systematic model study to investigate whether this type of internal variability can explain the observed mode water variability.

An eddy-resolving isopycnic primitive equation ocean model with idealized geometry is used. The ocean model has sufficiently high horizontal resolution for the energetic mesoscale eddies to be resolved. Because eddies are resolved, the explicit diffusion and viscosity (which parameterize subgrid-scale processes) are small. In this case, also internal low-frequency variability may be generated. The domain is small, which makes the model computationally efficient. The regional character of the present model enables us to do long integrations and perform many sensitivity experiments. In general, this study aims at understanding the processes and dynamics. The relatively simple configuration of the model allows us to focus on this.

This paper is organized as follows: in section 2 the numerical model, the forcing and the setup of the different experiments are discussed; section 3 describes the results of the control run and the different sensitivity experiments. In the last part of section 3 the results are discussed by studying results from idealized configurations of the model and by analyzing the thickness budget of the mode water layer. In section 4 a summary is given and conclusions are drawn.

2. Experimental Setup

2.1. Ocean Model

Observations show that diabatic effects in the interior of the ocean due to small-scale mixing are very small [e.g., *Ledwell et al.*, 1993]. The weak diabatic effects imply that in the interior of the ocean water is transferred almost adiabatically along isopycnal surfaces. This makes density a natural vertical coordinate for ocean models. Also the isopycnic layers can be related to water masses. Therefore isopycnic models are ideally suited for water mass studies. Here we use an isopycnic model that is based on the model of *Bleck and Boudra* [1986]. Various versions of the model have been used by *Drijfhout* [1994], *Drijfhout and Walsteijn* [1998] and *Hazeleger and Drijfhout* [1998, 1999, 2000]. We refer to these papers for details on the model. In the following the present model configuration will be described.

The model has seven isopycnic layers with a density difference of 0.8 kg m^{-3} between each layer (equivalent to a temperature difference of 4°C when salinity is kept constant). The deepest layer has a density of 1026.6 kg m^{-3} (i.e., an average temperature of 2°C at an average salinity of 35 practical salinity units (psu)), and a linear equation of state is used. In the remainder we will denote the isopycnic layers by their equivalent temperature, which is the average temperature a layer would have if the average salinity were 35 psu.

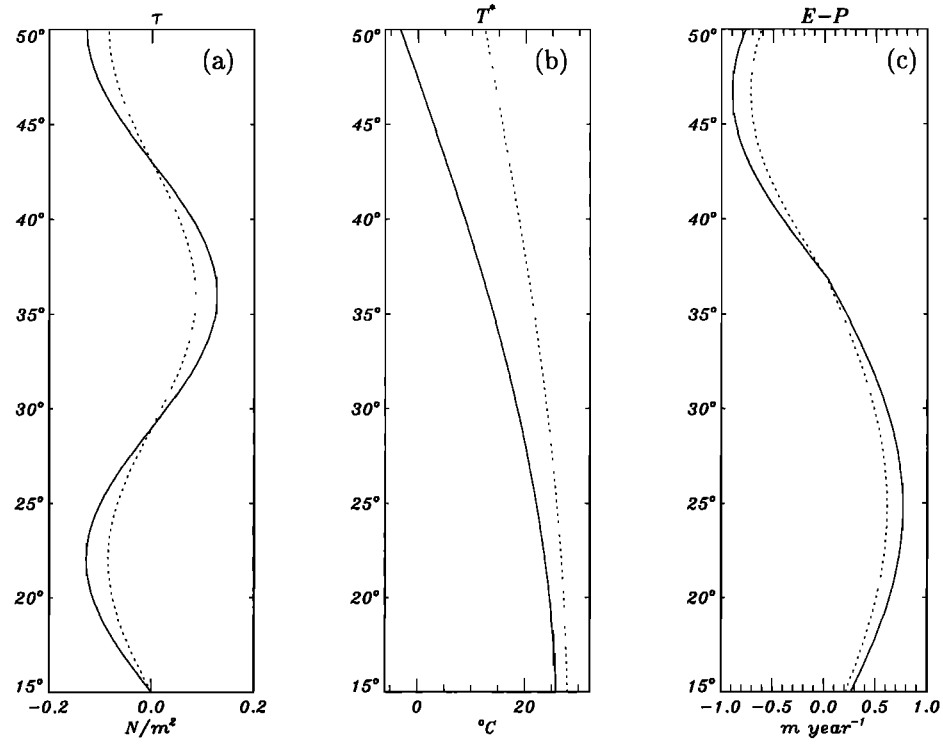

Figure 1. Zonally averaged forcing profiles (solid line, winter; dotted line, summer). (a) Wind stress, (b) apparent temperature, and (c) evaporation minus precipitation.

The model has a horizontal resolution of 37 km. Subgrid-scale processes are represented by a biharmonic friction and diffusion parameterization. The minimum value for the biharmonic diffusion and viscosity parameter is 1×10^{11} m^4 s^{-1} and a small diapycnic diffusion is included with a diffusivity of 1×10^{-4} m^2 s^{-1}. Under the present forcing (see next section) a vigorous eddy field can be simulated with this resolution and friction/diffusion parameterization. With a grid size smaller than 37 km the level of eddy kinetic energy and potential energy increases, but no qualitative changes occur with respect to the mesoscale eddies [*Drijfhout*, 1994].

The domain of the model is closed and describes an idealized North Atlantic midlatitude jet and the subtropical gyre. On the western side of the basin stepwise continental shelfbreak with a width of 500 km is incorporated [see *Drijfhout*, 1994].

As mixed layer processes are important in the formation of mode water, the isopycnic ocean model is coupled to a bulk mixed layer model. The mixed layer model is a Kraus-Turner mixed layer model based on the algorithm presented by *Bleck et al.* [1989]. This model is suitable because the vertical homogeneous structure of the isopycnal layers is retained in the mixed layer. Although more sophisticated mixed layer parameterizations are available, the bulk mixed layer model performs well considering the present idealized context (see *Hazeleger and Drijfhout* [1998] for a discussion). For more specific details on the algorithm we refer readers to *Bleck et al.* [1989].

2.2. Forcing

The ocean model was initialized from oceanic fields obtained after an extensive spinup of a coarse resolution version (dx = 74 km) of the model that had been used in a previous study [*Hazeleger and Drijfhout*, 1999]. The fields were interpolated to the fine resolution grid (dx = 37 km) used in this study. For the present fine resolution model we slightly changed the forcing profiles compared with those used in the coarse resolution model of *Hazeleger and Drijfhout* [1999]. This was done to reduce the overshoot of the Gulf Stream in the fine resolution model. The present forcing is shown in Figure 1. It consists of a zonally averaged varying wind stress and freshwater flux. As the horizontal resolution, the forcing, and the subgrid-scale parameterizations differ from the previous model run with the coarse resolution model, an additional spinup with the fine resolution model was necessary. In the first stage of the additional spinup, the sea surface temperature (SST) was restored to an apparent temperature. The apparent temperature differs from the atmospheric temperature in the boundary layer because it incorporates all contributions of the radiation budget [*Haney*, 1971]. The restoring timescale was 20 days for a mixed layer depth of 50 m, otherwise proportional to the mixed layer depth. The forcing varies sinusoidally between the extremes in the winter and summer as depicted in Figure 1. The negative freshwater flux is high in the north. In the subtropical gyre the evaporation is less than that observed. This is necessary to ensure a vanishing basin integrated freshwater flux.

Table 1. Experiments

Experiment	Friction/Diffusion	Coupling	$\mathcal{F}_\tau$
Control	biharmonic	yes	no
a	biharmonic	no	no
b	biharmonic	yes	no; no τ feedback
c	Laplacian	yes	no
d	Laplacian	yes	yes
e	biharmonic	no buoyancy forcing	yes; no mean forcing
f	biharmonic	no buoyancy forcing	no

The second column states the type of friction and diffusion parameterization that is used. The third column states whether the ocean model is coupled to the atmospheric anomaly model (if not, $Q'_H = 0$). The fourth column states whether stochastic forcing has been applied and gives additional information on the wind stress feedback. See text for further details.

As the basin width at the latitude of the maximum anticyclonic wind stress curl is about one third of the width of the subtropical Atlantic, the amplitude of the wind stress has been enhanced by a factor of 3 in comparison with observations. In this way, the linear component of the western boundary current will have the correct magnitude. The advective timescale of the subtropical gyre, however, becomes much too short after the wind enhancement (i.e., 1 to 2 years). To obtain a realistic ratio between advection and forcing time scales, the seasonal cycle is shortened by a factor of 3.

After 80 years a cyclo-stationary state was reached and the heat fluxes were diagnosed from the restoring boundary condition for temperature. Then the model was forced by an interpolated climatological heat flux $\overline{Q}$ plus an anomalous heat flux Q'_H. The climatological heat flux was calculated as an average of the monthly mean values of the last 20 years of the spinup. This is the heat flux the model "needs" to maintain a reasonable SST. Anomalous heat fluxes arise from SST anomalies and air temperature anomalies. Anomalous advective transports generate air temperature tendencies. These modify the mean heat flux, which in turn modifies SST and air temperature. Here the anomalous heat flux is determined from a bulk formulation. It depends on the difference between the anomalous SST (T'_{oc}) and anomalous air temperature (T'_a):

$$Q = \overline{Q} + Q'_H = \overline{Q} + \rho c_p C_H \epsilon |\mathbf{u}_a| (T'_a - T'_{oc}), \quad (1)$$

where $C_H = 1.3\times10^{-3}$ is the bulk transfer coefficient and T'_{oc} is the difference between the simulated SST and the SST diagnosed after the spinup. $\mathbf{u}_a$ is the wind speed, ρ is the air density, and c_p is the specific heat of air. The anomalous air temperature T'_a in the atmospheric boundary layer is determined with a prognostic equation, which includes advection, diffusion, and forcing ($-Q'_H$) of T'_a. This atmospheric anomaly model has been introduced by *Luksch and von Storch* [1992]. The heat flux consists of a sensible and latent heat flux. The ratio between both heat fluxes is 3 for oceanographic conditions [*Stull*, 1988]. Therefore ϵ, which is the ratio of the total heat flux to the sensible heat flux, is 4. In principle, SST anomalies are damped by the anomalous heat flux. In addition, the atmospheric anomaly model includes anomalous winds that are determined by applying the thermal wind equations to the air temperature anomalies [see *Hazeleger and Drijfhout*, (1999)]

The control run has been performed under control forcing. With this forcing, a circulation and water mass distribution is simulated that is typical for the subtropical North Atlantic. The results of this control experiment will be described in the next section. A number of sensitivity runs has been performed to clarify the physics of the low-frequency variability in the model. The different experiments are summarized in Table 1. The experiments are designed to study the effect of the coupling to the atmosphere and of the diffusion and friction parameterization on the variability. In section 3.2 the experiments are described and motivated in more detail.

3. Internal Variability

In the midlatitude jet region, high-frequency variability occurs, associated with mesoscale eddies. The eddies are generated by barotropic and baroclinic instability. Such high-frequency variability has been successfully simulated and studied in models with high resolution and low friction/diffusion. Here we will focus not on the high-frequency variability but on the larger-scale low-frequency variability. It will be studied how this type of internal variability is generated and whether it can play a role in the observed mode water variability.

We analyze the last 85 years of the model run described in the previous section. The 85 years are preceded by the spinup of 80 years. First, the linear trend of the last 85 years has been subtracted from the data. Then monthly anomalies were determined from the detrended data. A 1-year running mean has been performed to smooth the data and remove high-frequency variability. These data will be used to study the low-frequency variability. In addition, in the last 19 years of

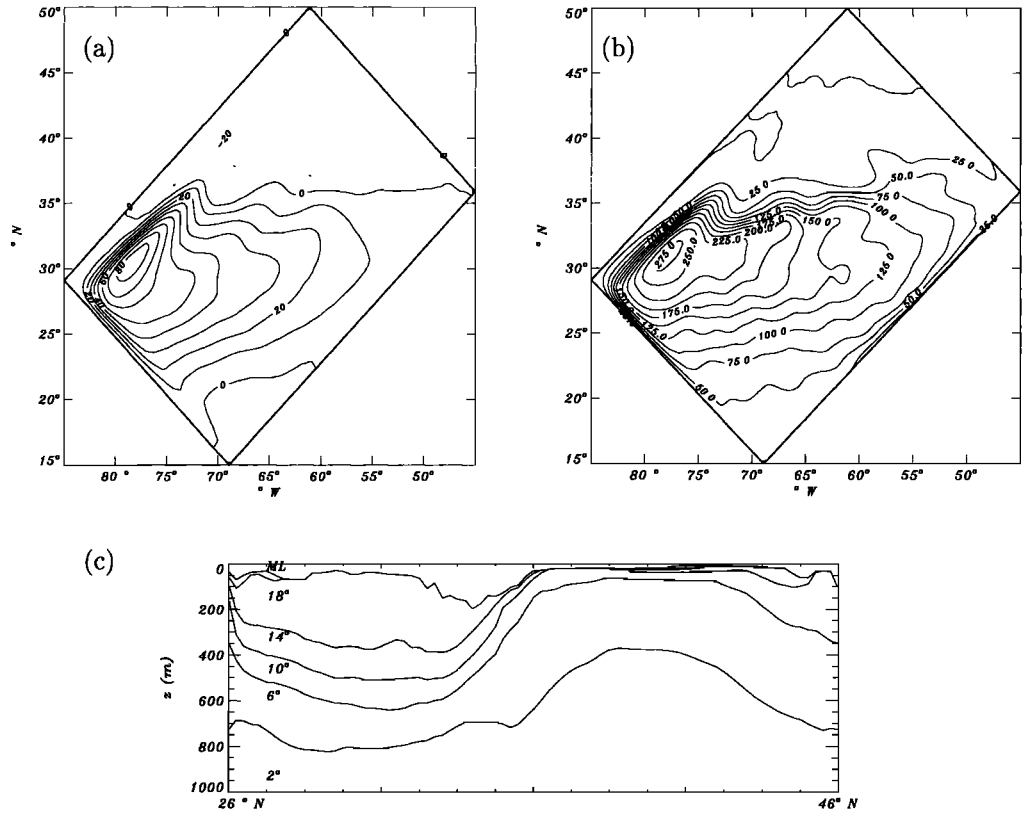

Figure 2. (a) Time-averaged barotropic streamfunction in Sverdrups (1 Sv = 10^6 m^3 s^{-1}). (b) Mean mode water thickness (in meters) in July. (c) Cross section showing isopycnal surfaces at he western side of the basin in July.

the control run, the mixed layer and mode water fields were saved every third day to assess mesoscale variability.

3.1. Control Experiment

In the control run the coupled model is used with a biharmonic friction parameterization (see Table 1). Although the model has been run for only 85 years after the spinup of 80 years, the run has not been continued as the low-frequency variability was very clear. First, we will show some basic characteristics of the simulated mean circulation.

Figure 2a shows the mean barotropic stream function. The large subtropical gyre and the smaller subpolar gyre are consistent with the geometry and the applied forcing. A tight Gulf Stream recirculation of 80 Sv is present. As the objective is to study mode water variability, mode water must be well represented in the model. Figure 2b shows the thickness of the 18°C layer in the model. It covers the entire subtropical gyre and is the model equivalent of mode water. The cross section in Figure 2c shows clearly that the 18°C layer is the thickest subsurface layer above the main thermocline. Also the typical bowl shape of the thermocline in the subtropical gyre is evident. Considering the idealized model configuration and forcing, the Atlantic subtropical circulation is well simulated. The variability in the 18°C layer is examined in this study.

The low-frequency variability displayed in the control run is substantial. Figure 3 shows a time-longitude diagram of (low-pass-filtered) thickness anomalies in the mode water layer of the model (the 18°C layer). The latitude is chosen to correspond with the latitude of the maximum thickness anomalies. These maxima are found at the westward return flow of the subtropical gyre, that is, at the southern edge of the mode water layer. However, it will be shown that the meridional scale of the anomalies is large enough to have a signature in a large part of the mode water layer. In Figure 3 we see large thickness anomalies propagating westward through the recirculation of the subtropical gyre. The spatial scale of the propagating anomalies shows that these anomalies do not correspond to the mesoscale eddies (which were filtered out).

In order to study spatial and temporal variability in the mode water layer in more detail, empirical orthonogal function (EOF) analysis is performed on the mode water thickness anomalies. The first, second, third, and fourth EOFs of mode water thickness account for 16%, 14%, 7% and 8% of the variance respectively. Almost all EOF patterns show wavelike features. The first and

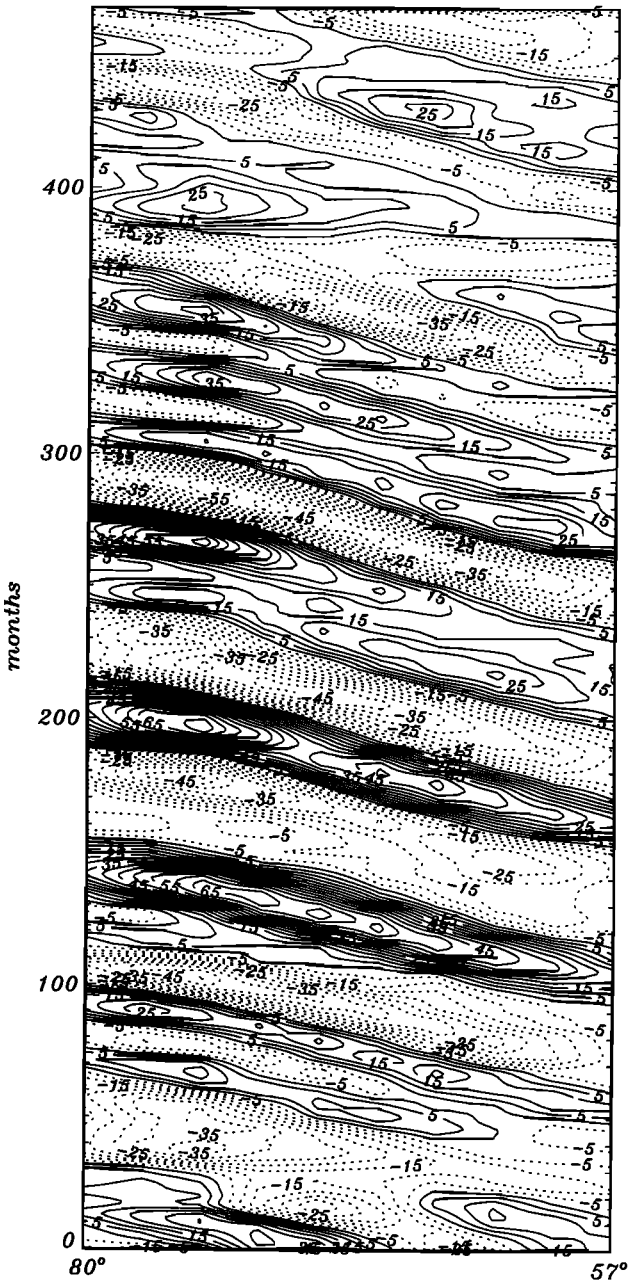

Figure 3. Time-longitude diagram at 25°N of low-pass-filtered thickness anomalies (in meters) in mode water.

the second EOF are in quadrature and describe a propagating feature. Together they explain 30% of the variance. EOF 3 and 4 also describe propagating thickness anomalies. The spatial patterns associated with the variability will be shown later in this section.

Spectra of the principal components of the first and fourth EOF are shown in Figure 4. The confidence intervals are based on 3000 spectra of first-order autoregressive processes (the idealized red noise response) with a variance and lag-one correlation of the unfiltered time series itself. The spectral power increases at lower frequencies and flattens off at the end. Above these background red noise spectra broad peaks arise, which imply dominant oscillatory behavior at these frequencies. The spectra of the first and second EOF peak around 8 years. The third and the fourth EOF peak at higher frequencies (around 4 years; see Figure 4).

The peaks in the spectra and the anomalies in the time-longitude diagram indicate propagation of thickness anomalies in the mode water layer. The EOF analysis can resolve only standing modes of variability. To quantify propagating modes, optimal autocorrelation function (OAF) analysis is more suitable [see *Hazeleger and Drijfhout,* 1999; *Selten et al.,* 1999]. OAF analysis maximizes the autocorrelation of a linear combinations of the time series of the EOFs. An oscillation can be represented if the eigenvalues of a pair of OAFs are in quadrature. The patterns of variability can be found by the linear combination of the associated OAF patterns (note that unlike EOFs, OAFs are not orthogonal and that they cannot be ordered by explained variance). Two propagating modes of variability are found by using the OAF analyses on the EOFs of mode water thickness. The timescales of the modes correspond to the timescales found in the spectra of the EOF time series. The spatial patterns of the two modes are depicted in Figure 5. The mode with a period of 8 years consists of large thickness anomalies that propagate westward. It appears that this OAF mode corresponds to the first and second EOF. The scale and the speed of the anomalies resemble those of the first baroclinic waves excited by stochastic wind stress in the coarse resolution version of the model [see *Hazeleger and Drijfhout,* 1999]. The amplitude of the variability in mode water thickness, however, is much higher in the present model. Here we find a maximum standard deviation of 40 m, compared with only 5 m in the coarse resolution model forced by a stochastic wind stress. The amplitude of the variability found here is of the order of the observed amplitude of variability [see *Talley,* 1996; *Molinari et al.,* 1997].

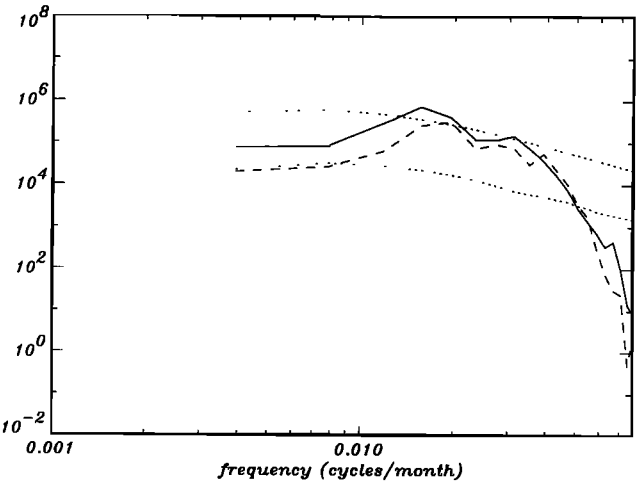

Figure 4. Spectrum of the principal components of the first (solid line) and fourth (dashed line) EOF of mode water thickness in the control experiment. Dotted lines are 95% confidence intervals.

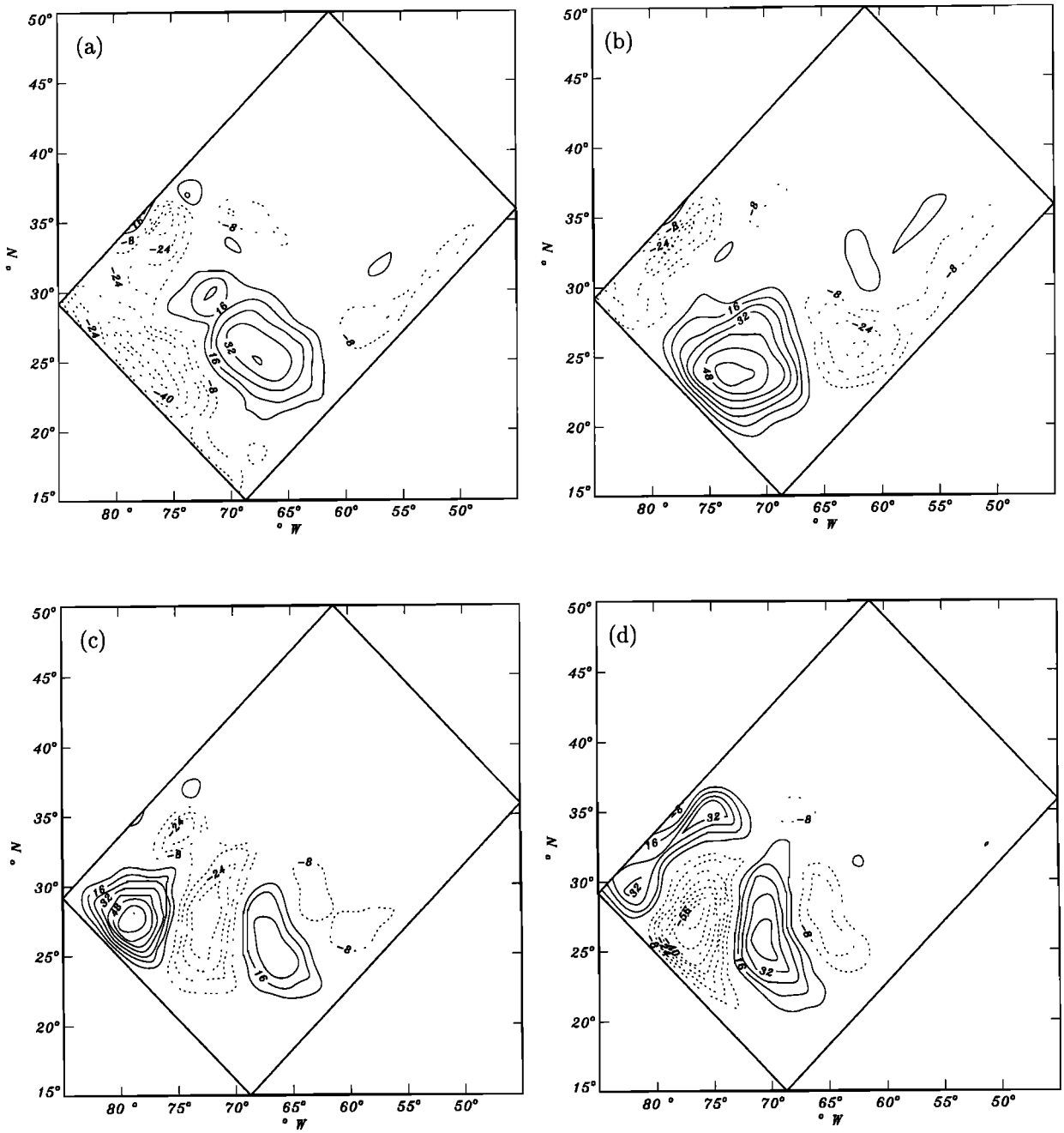

Figure 5. Anomalies in mode water thickness (in meters) derived from the OAF analysis. (a, b) Snapshots of the 8-year mode at 1/4 period apart. (c, d) Snapshots of the 4.5-year mode at 1/4 period apart.

The second mode with a shorter period also propagates westward. This mode contains the EOF 3 and 4 patterns. The spatial scale is smaller than that of the 8-year mode. The short period is the result of the smaller spatial scale. The propagation speed is equal to that of the 8-year mode. This can be observed in the time-longitude diagram of the filtered mode water thickness anomalies themselves (Figure 3). At different stages (for example, around the 80th month and around the 350th month) the small-scale and large-scale anomalies can be observed to have equal propagation speed. As the propagation speed is identical to the speed of the 8-year mode, the mode can not be a higher-order baroclinic mode. Apparently, this mode rides on the larger-scale mode.

The EOF analysis showed that 45% of the variance in the entire mode water layer, on all resolved timescales longer than 1 year, is explained by the propagating features that are recovered in the OAF analysis. Together with the significant peaks in the spectra, this implies that the low-frequency variability in mode water is dominated by the westward propagating thickness

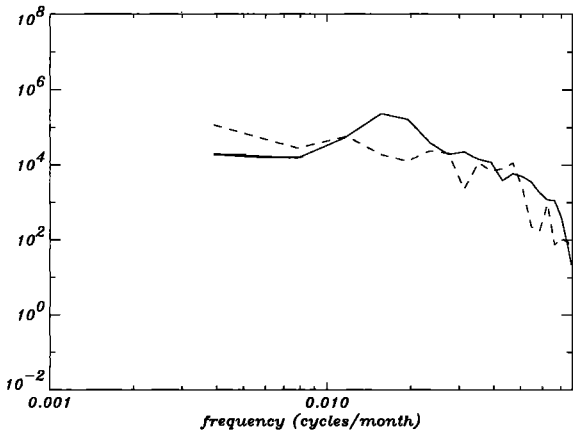

Figure 6. Spectra of principal components of the leading EOFs of mixed layer thickness. Spectra of first EOF control run (solid line) and of first EOF in experiment a, without thermal feedback (dashed line).

anomalies. The maximum amplitude of the variability is found at the thermocline where the vertical density gradient is large. The anomalies have primarily a first baroclinic modal structure. The thickness anomalies in the mode water layer (just above the thermocline) are compensated mainly in the layers beneath the thermocline (that is, the 6°C layer and the 2°C layer). Also the mixed layer thickness compensates partly (about 25%) for anomalies in the mode water layer. Although the maximum variability occurs at the southern edge of mode water, Figure 5 shows that the variability is found in a large part of the mode water layer.

The SST variability associated with the low-frequency variability in the subtropical gyre is significant. The maximum standard deviation is 2°C. This maximum is found at the separation point of the Gulf Stream. Here the warm subtropical and cold subpolar waters meet. The varying latitude of separation of the jet due to the internal variability leads to large SST variability here. Similar variability associated with variability in the separation point of the midlatitude jet has been found by, e.g., *Speich et al.* [1995] and *Jiang et al.* [1995] in simpler models and by *Brown and Evans* [1987] and *Hanson* [1991] in observations. In the subtropical gyre the standard deviation is 0.4°C. Observed SST variability ranges from 5°C in the Gulf Stream region to 3°C in the subtropical gyre [*Levitus et al.*, 1994]. This variability is generated by atmospheric variability (e.g., cooling by cold air outbreaks) and internal variability (that is, variability independent of atmospheric forcing). In the present model, hardly any atmospheric variability occurs (see section 3.2), except for the seasonal cycle. These results suggest that a large part of the SST variability in the Gulf Stream region is associated with internal variability. In the subtropical gyre, air-sea interaction is likely to play a more important role in generating SST variability.

3.2. Sensitivity Experiments

To gain insight in the physics of the variability displayed in the model, a suite of sensitivity experiments has been performed. The experiments are designed to assess the role of atmosphere-ocean coupling and the role of the strength of diffusion and friction. These sensitivity experiments can confirm whether the variability is truly internally generated. Some of the experiments are motivated by the results presented by *Hazeleger and Drijfhout* [1999]. There it was shown that low-frequency baroclinic waves could be excited by a stochastic wind stress in the coarse resolution version of the ocean-only model. Here similar waves are excited in the coupled eddy-resolving model under (nearly) constant forcing.

Table 1 summarizes the sensitivity experiments. All sensitivity runs have been run for 85 years. The first 10 years of each run are omitted in the analyses to allow the upper layers of the ocean to adjust to the different forcing.

3.2.1. Sensitivity to coupling to the atmosphere. In section 3.1 the variability displayed in, for example, Figure 3 is tentatively called internal variability. However, the atmospheric forcing in the control experiment is not constant. Variability induced by the coupling of the ocean to the atmosphere remains a possibility. Especially, the heat flux is allowed to vary in the coupled model (equation (1)). Also the wind stress can vary in response to air temperature anomalies. In this section we will study to what extent the observed variability is a coupled phenomenon and to what extent it is purely internal oceanic variability.

In the first sensitivity experiment (experiment a; see Table 1) the thermal feedback has been turned off ($Q'_H = 0$). So the buoyancy forcing of the model consists of heat and freshwater fluxes with a constant seasonal cycle. This experiment is designed to assess to what extent the oceanic variability is coupled to the atmosphere through SST-heat flux feedback.

As the atmospheric forcing has changed now, the model drifts to a different state. Water in the 18°C layer was lost to the 14°C layer, which became the thickest subsurface layer. Consequently, in experiment a the 14°C layer represents mode water. The oscillatory modes disappear in the 18°C layer but manifest themselves strongly in the 14°C layer now, consistent with the changed stratification. The subsurface thickness anomalies are still generated and have a similar structure as in the control run. So there are no qualitative differences between subsurface variability in the control run and in experiment a. The subsurface signal of the variability is not determined by this kind of coupling. However, the variability in the mixed layer is different in comparison with the control run. In the control run, the variability in mixed layer thickness is highly correlated with variability in the thermocline. In experiment a the spectra of the EOFs of mixed layer

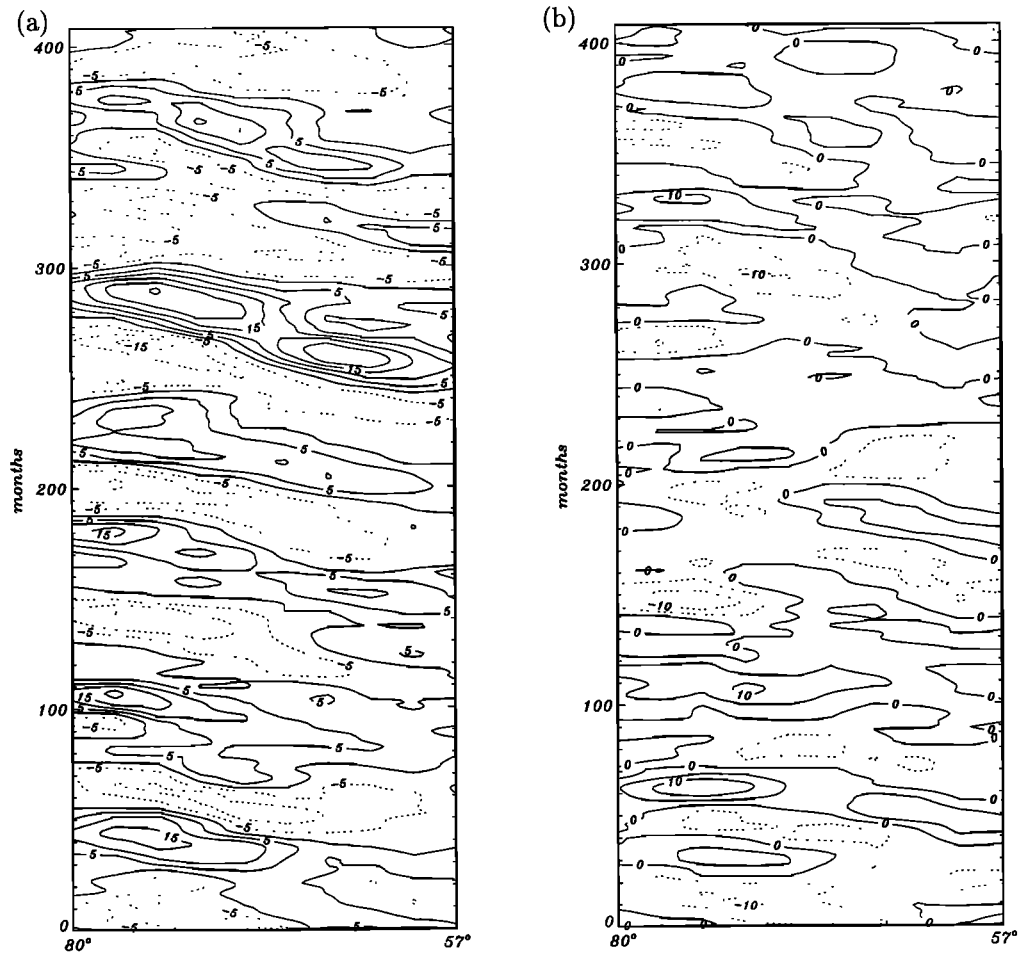

Figure 7. Time-longitude diagram along 25°N of low-pass-filtered mixed layer thickness anomalies (in meters). (a) Control experiment; (b) heat-flux-driven model (experiment a).

thickness do not show peaks (for example, first EOF in Figure 6). The variability is small and aperiodic. The compensation of changes in mode water thickness (now the 14°C layer) almost exclusively takes place below the thermocline. In the control run also compensation in the mixed layer occurs. Here the lack of compensation in the mixed layer (see Figure 7) must be caused by the absence of anomalous mixing induced by Q'_H. In the control run, the damping of SST anomalies by Q'_H (or any restoring heat flux parameterization) modifies the heat fluxes and therefore the turbulence kinetic energy (TKE) budget of the mixed layer. The anomalous heat fluxes affect entrainment/detrainment. This explains why the modes show up in the mixed layer when the model is coupled and disappear in the mixed layer when the model is driven by fixed heat fluxes. This experiment shows that there is no active SST-heat flux feedback.

In some coupled ocean-atmosphere models, coupled instabilities have been found associated with an SST-wind stress feedback [e.g., *Latif and Barnett*, 1996]. In Latif and Barnett's case, the SST variations in the North Pacific induce variability in the atmospheric winds. The ocean, in turn, adjusts to these winds by a spinup of the subtropical gyre. In the present model the SST anomalies feed back on the wind stress anomalies by the thermal wind relation. To test whether this feedback is important, the wind anomalies have been set to zero in experiment b. The same modes as those found in the control experiment are found again (not shown). This implies that a coupled instability such as that suggested by *Latif and Barnett* [1996] is not acting in our model. Together with the lack of SST-heat flux feedback this rules out that the present modes are coupled modes. They should be interpreted as internal ocean-only modes.

3.2.2. Sensitivity to friction and diffusion. In the previous section we have shown that low-frequency variability in the model's mode water is not associated with the atmospheric forcing. This type of internal variability is not generated in coarse resolution ocean models that are usually used for climate studies. So there must be processes in the eddy-resolving model that are absent in the coarse resolution model that are responsible for the variability to be excited. The strength of the friction and diffusion is the main candidate. Strong

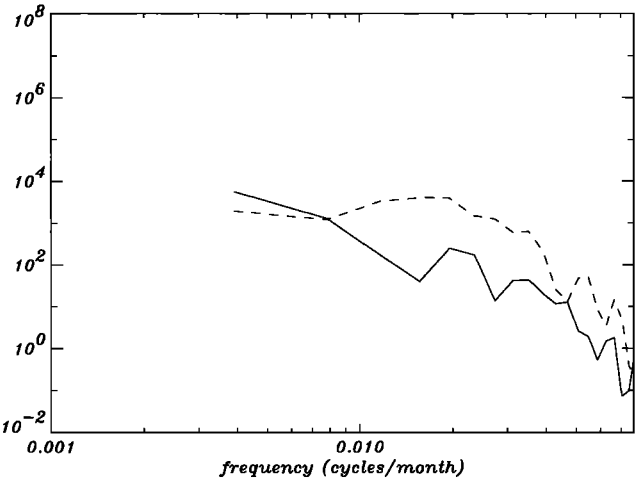

Figure 8. Spectrum of the principal components of the first EOF of mode water thickness in experiment c where high Laplacian friction is used (solid line) and of the first EOF of mode water thickness in experiment d where a stochastic wind stress is added (dashed line).

diffusion and friction parameterizes mesoscale eddies in coarse resolution models. As eddies are resolved in high-resolution models, the diffusion and friction can be reduced.

To study the role of the strength of friction and diffusion, a strong Laplacian friction and diffusion are used instead of the weak biharmonic friction and diffusion in the control run (experiment c). The harmonic friction parameter is 3000 m^2 s^{-1}, and the diffusivity parameter is 1500 m^2 s^{-1}. These values are identical to the values in the coarse resolution version of the model [see *Hazeleger and Drijfhout*, 1999]. At these high values, no mesoscale eddies are generated. No low-frequency variability arises as well, in contrast to the control experiment where horizontal mixing is carried out by the eddies generated by baroclinic instabilities (see Figure 8; owing to small drift, the spectrum does not flatten yet).

Whether the low-frequency variability is excited appears to depend critically on the strength of the diffusion. A short (20-year) sensitivity experiment with strong diffusion and weak viscosity showed that the modes were damped, while in an experiment with weak diffusion and strong viscosity the modes were unaffected. The thickness diffusion acts to flatten the slope of isopycnals. Apparently, this process damps the anomalies. The instability characteristics of the ocean circulation are determined by the slopes of the isopycnals. Large viscosity has no direct impact on the slopes of the isopycnal surfaces.

3.2.3. Relation between internal and stochastically forced variability. Although strong diffusion prevents the instabilities from growing, variability similar to that shown here can be excited by stochastic wind stress in a coarse resolution model with strong diffusion [*Hazeleger and Drijfhout*, 1999]. We have tested whether the stochastic wind stress can excite the low-frequency variability in the fine resolution model with high friction and diffusion (experiment d).

The stochastic wind stress has a decorrelation timescale of 7 days, a standard deviation of 0.1 N m^{-2}, and a varying coherent spatial scale [see *Hazeleger and Drijfhout*, 1999], i.e.,

$$\mathcal{F}_\tau(x,y,t) = \sum_{i=1}^{2}\sum_{j=1}^{3} Z_{ij}(t)\sin\left(\frac{ix\pi}{L_x}+\phi_{ij}(t)\right) \times \sin\left(\frac{jy\pi}{L_y}+\phi_{ij}(t)\right); \quad (2)$$

here $\mathcal{F}_\tau$ is the additional stochastic wind stress forcing, L_x is the zonal extension of the domain, L_y is the meridional extension of the domain, Z is a random amplitude, and ϕ is a random phase. The stochastic forcing mimics the propagating synoptic disturbances. On average, the patterns are sinusoidal, which mimics the NAO and a few higher harmonics.

Indeed, low-frequency variability is generated (see Figure 8). The peaks in the EOFs of mode water thickness are very broad. The EOF patterns clearly show the wavelike features, resembling those found in the work of *Hazeleger and Drijfhout* [1999] (not shown). The spatial scale of the thickness anomalies is rather large, suggesting that only the 8-year mode is excited by the stochastic wind stress. The maximum standard deviation of mode water thickness is only 6 m. *Hazeleger and Drijfhout* [1999] found an amplitude of 5 m. Note that this amplitude is much lower than that observed.

Apparently, the stochastic forcing can sustain the 8-year mode in the model which would be damped otherwise by the strong diffusion. Therefore this variability in the model's mode water seems to consist of damped oscillatory eigenmodes of the ocean itself (see section 3.3 for a discussion). The 4.5-year mode is still damped; it may get excited at a higher Reynolds number, or it may be forced less efficiently, as the large-scale stochastic wind stress projects better on the larger-scale mode.

3.3. Free and Wind-Driven Modes of Variability

We have shown that the variability in the model is internally generated, but it is not yet clear by what mechanism this takes place. In experiment c it has been shown that no mesoscale eddies and no low-frequency variations were generated when the diffusion was strong. It remains unclear whether the diffusion itself is responsible for damping the variability, either directly or indirectly by affecting the slope of isopycnals associated with the midlatitude jet, or if the presence of the mesoscale eddies is essential. The mesoscale eddies can feed energy into the low-frequency variability, and they can act as a source of stochastic noise that excites the variability. Therefore we will explore whether the mean flow (i.e., sloping isopycnals) is critical for generating the low-frequency variability.

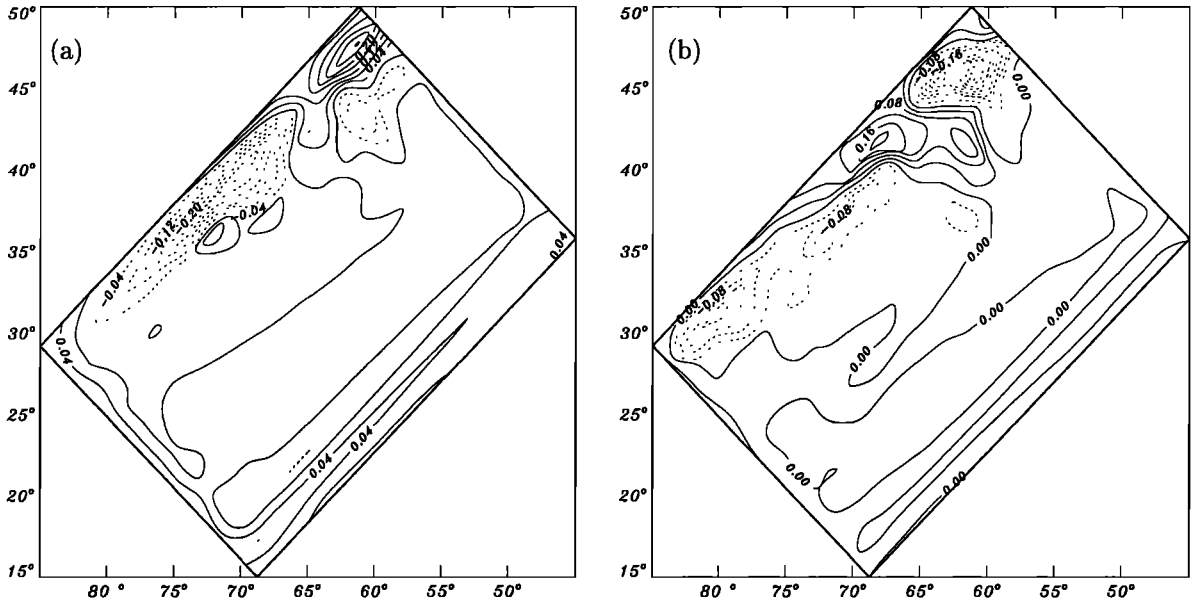

Figure 9. EOF patterns of mode water thickness in experiment e. (a) First EOF (explained variance, 33%); (b) second EOF (explained variance, 22%).

In the previous section we suggested that the low-frequency internal variability in the present model is an instability of the mean flow (i.e., not related to the mesoscale eddies). When the mean flow is weak, it probably consists of two damped eigenmodes of the system which can be excited by noise. When the mean flow is strong, it becomes unstable for these two modes. We have performed two experiments to test this hypothesis. As the gyres are primarily wind driven we will assume that thermodynamics do not play a role in generating the variability. Therefore from now on we will use the isopycnic ocean model (i.e., no mixed layer and no coupling to the atmosphere). Only the adiabatic layer thickness equation and the momentum equations are solved. This model is purely wind driven and has the same basin geometry, topography, and parameterization of subgrid-scale processes as in the control experiment.

In the first experiment (experiment e) we force the adiabatic model with a stochastic (zero mean) wind stress only, to determine the free modes of the system associated with the basic stratification. These will act as a reference for the next experiment. In that experiment we force the adiabatic model with a constant wind stress (experiment f) and investigate whether the variability resembles that found in the control experiment. Furthermore, we study to what extent the variability is associated with the free modes, and to what extent the instability of the mean flow determines the observed variability.

In experiment e the model is initialized with horizontally constant layer thicknesses. In this configuration there can be no mean flow. The depth of the isopycnal interfaces correspond to the average depth of the isopycnals along 27°N in the control experiment. At this latitude the anomalies in mode water are strongest. With this experiment we intend to find the free modes of the system associated with the basic stratification.

In Figures 9a and 9b we show the first and the second EOF of the mode water layer in experiment e. The EOFs are in quadrature and reflect the spatial structure of propagating anomalies in the mode water layer. The response consists of anomalies which eminate from the eastern boundary. Some anomalies propagate westward across the basin from the eastern boundary toward the western boundary. These are baroclinic waves. The speed of the anomalies is higher toward the south owing to the changes in the Coriolis parameter. This response is consistent with the simple linear stochastic forcing model presented by *Frankignoul et al.* [1997]. Other, faster signals propagate counterclockwise along the boundary. These anomalies can be identified as Kelvin waves. The anomalies become more pronounced at the continental shelf break at the western boundary. Upon arrival of the Kelvin wave signal at the eastern boundary, a new Rossby wave signal is initiated. This determines the timescale of 13 years which was found in the spectra and OAF analysis (not shown). The amplitude is very small; the standard deviation of mode water thickness in the southeastern part of the basin is about 1 m. The spatial scale and the amplitude of the low-frequency variability bears no resemblance with the modes found in the control experiment. Also the amplitude is much smaller. Apparently, the variability in the control experiment is not associated with these free modes of the ocean basin.

In the second experiment we have forced the model with a constant mean (wintertime) wind stress (experiment f). As the thermodynamics damps the flow, the amplitude of the wind stress has been reduced by a

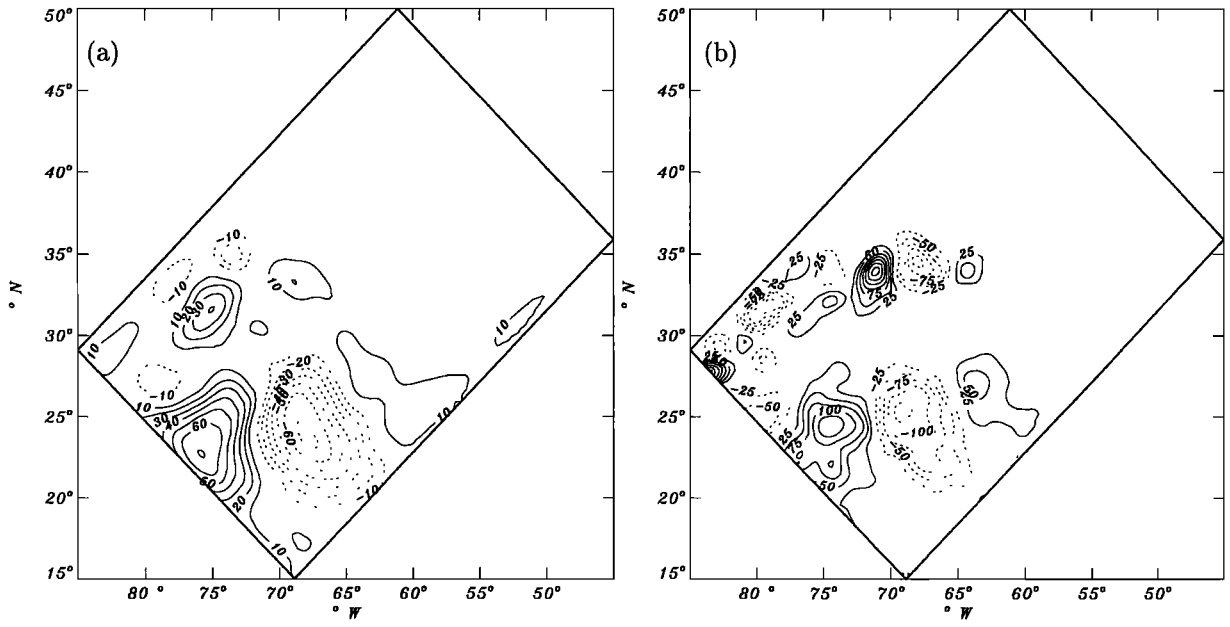

Figure 10. (a) Tendency of anomalous mode water thickness associated with the low-frequency variability ($\partial h^*/\partial t$). (b) Pattern of the left hand side terms in equation (4) that project well on the evolution of the low-frequency variability, i.e., $-\nabla \cdot [\overline{(\overline{\mathbf{u}}h^*)}^{yr} + \overline{(\mathbf{u}^*\overline{h})}^{yr}]$. Values are expressed in meters per year.

factor of 2. With this forcing, the velocities in the surface layer are comparable to the velocities in the control experiment. The model was initialized with the mean wintertime stratification derived from the control experiment. Now the stratification contains the slope of the midlatitude jet.

In experiment f also westward propagating modes are found. The low-frequency variability resembles the variability found in the control experiment. The amplitude, spatial scale, and timescale are similar. Although these anomalies may have the same nature as the free modes found in experiment e, they are strongly modified by the mean flow and the stratification. In experiment f also Kelvin waves are observed to propagate from the east along the northern and western boundary, but they dissipate before reaching the southern boundary. Spectra of EOFs in experiment f show only peaks around 4 and 8 years. This sensitivity experiment shows that the characteristics of the instabilities depend on details in the stratification (sloping isopycnals). We suggest that both modes can be regarded as instabilities of the mean flow.

3.4. Thickness Budget

In the previous section we have established that the characteristics of the variability displayed in the control experiment depend on the mean flow. In this section we explore whether the amplitude of the low-frequency mode water variability is determined by feedback between the eddies and the low-frequency variability or whether it is determined by interaction between the mean flow and low-frequency variability. For this purpose we analyze the thickness budget of the mode water layer. To this end, an energy budget analysis might have been more appropriate, but owing to the presence of three or even four components (if the two modes are treated separately), this would be extremely elaborative and beyond the scope of this paper.

The thickness and velocity are decomposed in a climatological mean, a high-frequency (that is, mesoscale eddies) and a low-frequency (that is, the baroclinic waves) component; i.e., for any variable x,

$$x = \overline{x} + x' + x^*. \tag{3}$$

Three timescales are involved in this decomposition: the high-frequency eddy timescale (of the order of days to weeks); the climatological mean timescale (of the order decades; note that it resolves a constant seasonal cycle); and the timescale of the modes (of the order of order months to years). Anomalies are split into an eddy component (x') and a mode component (x^*). The latter are obtained from projecting the modes (OAF) on the anomalous fields. We analyze the thickness budget on a time span of 1 year because this timescale resolves the slower evolution (growth and decay cycle) of the low-frequency variability while it smoothes the high-frequency noise. Moreover, by choosing exactly 1 year, the tendency of the mean flow (i.e., the seasonal cycle) vanishes. The layer thickness equation becomes

$$\frac{\partial \overline{h^*}^{yr}}{\partial t} + \frac{\partial \overline{h'}^{yr}}{\partial t} = -\nabla \cdot \overline{(\overline{\mathbf{u}}\overline{h} + \mathbf{u}'h' + \mathbf{u}^*h^* + \overline{\mathbf{u}}h' + \mathbf{u}'\overline{h} + \overline{\mathbf{u}}h^* + \mathbf{u}^*\overline{h} + \mathbf{u}^*h' + \mathbf{u}'h^*)}^{yr} + \overline{\mathcal{S}}^{yr}. \tag{4}$$

Table 2. Values of the Basin-Integrated (Angle Brackets) Contribution of the Projection of the Terms in Equation (4) on the Tendency of the Low-Frequency Variability (h_t^*, Figure 10a)

Expression	Value
$<h_t^* h_t^*>$	310
$<h_t^* h_t'>$	18
$<h_t^* \nabla(\mathbf{u}^* h^*)>$	-2
$<h_t^* \nabla(\mathbf{u}' h')>$	-34
$<h_t^* \nabla(\overline{\mathbf{u}}\overline{h})>$	133
$<h_t^* \nabla(\mathbf{u}^* \overline{h})>$	71
$<h_t^* \nabla(\overline{\mathbf{u}} h^*)>$	-471
$<h_t^* \nabla(\mathbf{u}^* h')>$	4
$<h_t^* \nabla(\mathbf{u}' h^*)>$	-16
$<h_t^* \nabla(\mathbf{u}' \overline{h})>$	72
$<h_t^* \nabla(\overline{\mathbf{u}} h')>$	-69
$<h_t^* \mathcal{S}>$	-36

The values are averaged over 1 year and divided by the number of grid points in the domain to get values expressed in $m^2\ yr^{-2}$.

Here $\mathbf{u} = (u, v)$, h is the layer thickness, and $\mathcal{S}$ comprises the diapycnal mass fluxes (entrainment/detrainment) and layer thickness diffusion. Budget analysis showed that diffusion does not play a role. The anomalous velocity $\mathbf{u}^*$ is obtained from the anomalous geostrophic flow:

$$\mathbf{u}^* = \frac{g'}{f}\mathbf{k} \times \nabla h^*. \tag{5}$$

This can be justified by the large spatial scale of the anomalies ($\mathcal{O}$ (1000 km)) and the small velocities ($\mathcal{O}$ (5 $\times 10^{-2}$ m s^{-1})).

The horizontal distributions of the terms in equation (4) are multi-signed. Also the contribution of the eddy thickness tendency ($\partial \overline{h'}^{yr}/\partial t$) is still substantial, which obscures the interpretation of the spatial patterns. To examine which terms contribute to the evolution of the low-frequency variability, we analyzed the covariability of the terms in equation (4) with the propagating modes themselves. This was done by projecting the terms in equation (4) on the thickness tendency of the modes ($\partial \overline{h^*}^{yr}/\partial t$, see Figure 10a). That is, we calculated the basin integral of each term in equation (4) multiplied by $\partial \overline{h^*}^{yr}/\partial t$. The results are shown in Table 2.

From Table 2 it is clear that the largest contributor to the evolution of the low-frequency variability is the differential advection by the mean flow ($\nabla(\overline{\mathbf{u}}h^*)$). The contributions of the terms that involve a correlation between the eddies and the mode, $\nabla(\mathbf{u}^* h')$ and $\nabla(\mathbf{u}' h^*)$, are small. Also the self-interaction terms are small. As the mode-mode interaction ($\nabla(\mathbf{u}^* h^*)$) is small, we did not pursue an analysis of the interactions between the 4.5- and the 8-year mode. $\mathcal{S}$ comprises mass fluxes by entrainment/detrainment and friction/diffusion. As was stated before, the friction and diffusion are small in the present model. The small contribution of entrainment/detrainment implies that the interaction between the mixed layer and the subsurface layers does not contribute to the propagating mode. This is consistent with results of the sensitivity experiments.

These results show that the evolution of the low-frequency variability is determined mainly by an interaction between the modes and the mean flow. Convergence or divergence due to mass fluxes associated with advection of the anomalies by the mean flow primarily sustains the modes. This reflects the instability of the mean flow to these anomalies. The contribution to the thickness budget of the interaction terms between low-frequency variability and mean flow is shown in Figure 10b. As would be expected, these terms correlate well with the evolution of the low-frequency variability itself (Figure 10a). As the amplitude is lower in Figure 10a than in Figure 10b, the other terms (on the average) act to damp the modes.

So the low-frequency variability in mode water is not directly excited by the eddies. A short sensitivity experiment where the layer thicknesses in the coarse resolution model were stochastically perturbed with a first baroclinic modal vertical structure and a horizontal structure on the eddy scale confirmed this. No (quasi) periodic variability was found. This supports our hypothesis that the low-frequency variability consists of two eigenmodes of the system which are damped when high diffusion causes the slopes of the isopycnic surfaces associated with the midlatitude jet to be subcritical. When the diffusion is reduced, both modes are no longer damped, and they can evolve as the mean flow gets unstable and feeds energy into these modes.

4. Summary and Conclusions

Observations show interannual to decadal variability in subtropical mode water formation [*Talley and Raymer*, 1982; *Dickson et al.*, 1996; *Molinari et al.*, 1997; *Suga and Hanawa*, 1995]. This low-frequency variability in subtropical mode water formation cannot be entirely generated by local atmospheric forcing [*Jenkins*, 1982; *Talley and Raymer*, 1982; *Talley*, 1996; *Yasuda and Hanawa*, 1997; *Suga and Hanawa*, 1995]. As the variability is not generated by atmospheric forcing alone, internally generated ocean variability may also play a role. This possibility has been investigated in this study. A numerical eddy-resolving ocean model coupled to an atmospheric anomaly model has been used for this purpose. In this model, strong low-frequency internal variability arises. It is characterized by westward propagating anomalies through the westward return flow of the subtropical gyre with amplitudes up to 50 m.

Two significant modes of variability are found in the model's equivalent of mode water: one with a 8-year period and a large spatial scale (wavelength of 2500 km) and another with a 4.5-year period and a smaller

scale (wavelength of 1200 km). These time scales are within the range of the observed timescale of variability in mode water formation. The propagation speed of both modes is identical ($\approx$4.5 cm s^{-1}). The speed is about equal to the phase speed of the first baroclinic Rossby wave.

In the numerical model, the low-frequency variability arises even when the ocean-only model is forced by fixed wind stresses alone. So the low-frequency variability consists of (internal) ocean-only modes. In the present model, no unstable coupled mode arises. The absence of a coupled ocean-atmosphere instability may be due to the simplicity of the atmospheric anomaly model. The model does include some essential feedback but lacks atmospheric dynamics. The low-frequency variability has a maximum amplitude at the thermocline. Even without coupling to the atmosphere these modes arise. However, in this case variability in the mixed layer becomes aperiodic and does not correlate with variability in the thermocline. Apparently, coupling induces a feedback that generates an imprint of the subsurface variability in the mixed layer due to anomalous entrainment/detrainment.

The largest mode of low-frequency variability is also present in the coarse resolution version of the model when it is forced with a stochastic wind stress. This suggests that it is a preferred mode in the model that is damped when diffusion causes the isopycnal slopes in the midlatitude jet to be subcritical. Excitation of damped oscillatory modes by stochastic noise has been clarified by *Griffies and Tziperman* [1995]. When the diffusion is small, the mode is no longer damped and an interaction between the mode and the mean flow determines its evolution. This appears to be determined mainly by differential advection of the low-frequency thickness anomalies by the mean flow. The smaller-scale mode was not excited by stochastic noise. It can be associated with an instability that occurs at a higher Reynolds number. Also the stochastic wind stress may project better on the basin-scale mode than on the smaller-scale mode. To clarify this more precisely, as well as the exact mechanism by which the low-frequency variability is excited, a systematic bifurcation study should be performed in a comparable, but simplified, model.

The variability in mode water in the model has similar characteristics as the observed variability. *Molinari et al.* [1997] show excursions of the 18°C isotherm of at least 50 m on the decadal timescale (see their Figures 7 and 8). Equivalent potential vorticity changes have been shown by *Talley and Raymer* [1982] and *Talley* [1996]. Thickness variations in the mode water layer of the model have a similar amplitude (Figure 3). The observed anomalies are smaller in the surface layers than at the thermocline. This is consistent with results found in the model where thickness anomalies in mode water are mainly compensated by thickness anomalies below the thermocline and less by those in the surface layers. Also baroclinic waves on interannual to decadal timescales are found in the observations. The spectrum of the sea level at Bermuda shows enhanced energy around 3-4 years and 6-7 years [*Sturges and Hong*, 1995]. These variations have been explained in terms of first baroclinic mode Rossby wave propagation. *Sturges et al.* [1998] show that the Rossby wave propagation speed is 4 cm s^{-1} at 24°N. This is within the range of the propagation speed found in the model. Rossby wave propagation is also clear from altimetry [*Polito and Cornillon*, 1997]. In the North Pacific, propagation of subsurface thermal anomalies has been observed in the thermocline (e.g., Figure 14 of *Zhang and Levitus* [1997]). *Tourre et al.* [1999] notice that westward propagating heat content anomalies in the North Pacific follow the shear of the North Equatorial Current at 200-400 m. This feature is also present in the mode water layer of the numerical model. Note that the internal variability is strongest in the southwestern part of the basin. In this region, *Yasuda and Hanawa* [1997] found a weak covariability between variability in atmospheric forcing and mode water variability.

A large part of the observed mode water variability is probably forced by atmospheric variability [*Dickson et al.*, 1996; *Suga and Hanawa*, 1995; *Hazeleger and Drijfhout*, 1998]. However, there are inconsistencies between variability in the atmospheric forcing and variability in mode water. The characteristics of internal variability in the model suggest that this may be explained by internal ocean variability. However, the present model is very idealized, and other processes (e.g., nonlocal feedback, coupled instabilities) cannot yet be ruled.

Acknowledgments. We thank Will de Ruijter for his valuable comments on this manuscript. We also thank the reviewers for their comments. This work has been supported by Netherlands Organization of Scientific Research (NWO), project 770-03-252. Computations have been performed on the Fujitsu vpp700 of ECMWF, Reading.

References

Bleck, R., and D. B. Boudra, Wind-driven spin-up in eddy-resolving ocean models formulated in isopycnic and isobaric coordinates, *J. Geophys. Res., 91,* 7611-7621, 1986.

Bleck, R., H. P. Hanson, D. Hu, and E. B. Kraus, Mixed layer-thermocline interaction in a three-dimensional isopycnic coordinate model, *J. Phys. Oceanogr., 19,* 1417-1439, 1989.

Brown, O. B., and R. H. Evans, Satellite infrared remote sensing, in *Study of Physical Processes on the U.S. Mid-Atlantic Slope and Rise*, IV-67-IV-97, edited by C. Casagrande, Science Appl. Int., Raileigh, NC, 1987.

Cayan, D., Latent and sensible heat flux anomalies over the northern oceans: Driving the sea surface temperature, *J. Phys. Oceanogr., 22,* 541-560, 1992.

Cox, M. D., An eddy resolving numerical model of the ventilated thermocline: Time dependence, *J. Phys. Oceanogr., 17,* 1044-1056, 1987.

Deser, C., M. A. Alexander, and M. S. Timlin, Upper-ocean thermal variations in the North Pacific during 1970-1991, *J. Clim., 9,* 1840-1855, 1996.

Dickson, R., J. Lazier, J. Meincke, P. Rhines, and J. S. Swift, Long-term coordinated changes in the convective activity of the North Atlantic, *Prog. Oceanogr., 38,* 241-295, 1996.

Drijfhout, S. S., Heat transport by mesoscale eddies in an ocean circulation model, *J. Phys. Oceanogr., 24,* 353-369, 1994.

Drijfhout, S. S. and F. H. Walsteijn, Eddy-induced heat transport in a coupled ocean-atmospheric anomaly model, *J. Phys. Oceanogr., 28,* 250-265, 1998.

Frankignoul, C., P. Müller, and E. Zorita, A simple model of the decadal response of the ocean to stochastic wind forcing, *J. Phys. Oceanogr., 27,* 1533-1546, 1997.

Griffies, S. M., and E. Tziperman, A linear oscillator driven by stochastic atmospheric forcing, *J. Clim., 8,* 2440–2453, 1995.

Haney, L. R., Surface thermal boundary condition for ocean circulation models, *J. Phys. Oceanogr., 1,* 241-246, 1971.

Hanson, H. P., Climatological perspectives, oceanographic and meteorological, on variability in the subtropical convergence zone in the northwestern Atlantic, *J. Geophys. Res., 96,* 8517-8529, 1991.

Hasselmann, K. , Stochastic climate models, part I, Theory, *Tellus, 28,* 473-485, 1976.

Hazeleger, W., and S. S. Drijfhout, Mode water variability in a model of the subtropical gyre; Response to anomalous forcing, *J. Phys. Oceanogr., 28,* 266-288, 1998.

Hazeleger, W., and S. S. Drijfhout, Stochastically forced mode water variability, *J. Phys. Oceanogr., 29,* 1772-1786, 1999.

Hazeleger, W., and S. S. Drijfhout, Eddy-subduction in a model of the subtropical gyre, *J. Phys. Oceanogr., 30,* 677-695, 2000.

Jenkins, W. J., On the climate of a subtropical gyre: Decade timescale variations in water mass renewal in the Sargasso Sea, *J. Mar. Res., 40,* suppl., 265-290, 1982.

Jiang, S., F. F. Jin, and M. Ghil, Multiple equilibria, periodic, and aperiodic solutions in a wind-driven, double gyre, shallow-water model, *J. Phys. Oceanogr., 25,* 764-786, 1995.

Joyce, T. M., and P. Robbins, The long term hydrographic record at Bermuda, *J. Clim., 9,* 2407-2423, 1996.

Latif, M., and T. P. Barnett, Decadal climate variability over the North Pacific and North America: Dynamics and predictability, *J. Clim., 9,* 2407-2423, 1996.

Ledwell, J. R., A. J. Watson, and C. S. Law, Evidence for slow mixing across the pycnocline from an open-ocean tracer-release experiment, *Nature, 364,* 701-703, 1993.

Levitus, S., T. P. Boyer, and J. Antonov, *World Ocean Atlas,* vol. 5, *Interannual Variability of the Upper Ocean Thermal Structure, NOAA Atlas NESDIS 5,* 176 pp., U.S. Gov. Print. Off., Washington, D.C., 1994.

Luksch, U., and H. von Storch, Modelling low-frequency sea surface temperature variability in the North Pacific, *J. Clim., 5,* 893-906, 1992.

Marsh, R., and A. L. New, Modelling 18° water variability, *J. Phys. Oceanogr., 26,* 1059-1080, 1996.

Masuzawa, J., Subtropical mode water, *Deep Sea Res. Part I, 16,* 463-472, 1969.

Molinari, R. L., D. A. Mayer, J. F. Festa, and H. F. Bezdek, Multiyear variability in the near-surface temperature structure of the midlatitude western North Atlantic Ocean, *J. Geophys. Res., 102,* 3267-3278, 1997.

Polito, P. S., and P. Cornillon, Long baroclinic Rossby waves detected by TOPEX/POSEIDON, *J. Geophys. Res., 102,* 3215-3235, 1997.

Qiu, B., and R. X. Huang, Ventilation of the North Atlantic and North Pacific: subduction versus obduction. *J. Phys. Oceanogr., 25,* 2374-2390, 1995.

Selten, F. M., R. J. Haarsma, and J. D. Opsteegh, North Atlantic decadal variability in a climate model of moderate complexity, *J. Clim., 12,* 1956-1973, 1999.

Speich, S., H. Dijkstra, and M. Ghil, Successive bifurcations in shallow-water model applied to the wind-driven ocean circulation, *Nonl. Proc. Geoph., 2,* 241–268, 1995.

Stull, R. B. *An Introduction to Boundary Layer Meteorology,* 666 pp., Kluwer Acad., Norwell, Mass., 1988.

Sturges, W., and B. G. Hong, Wind forcing of the Atlantic thermocline along 32°N at low frequencies, *J. Phys. Oceanogr., 25,* 1706-1715, 1995.

Sturges, W., B. G. Hong, and A. J. Clarke, Decadal wind forcing of the North Atlantic subtropical gyre, *J. Phys. Oceanogr., 28,* 659-668, 1998.

Suga, T., and K. Hanawa, Interannual variations of North Pacific subtropical mode water in the 137-degree-E section, *J. Phys. Oceanogr., 25,* 1012-1017, 1995.

Talley, L. D., North Atlantic circulation and variability, reviewed for the CNLS conference, *Phys. D, 98,* 625-646, 1996.

Talley, L. D., and M. E. Raymer, Eighteen degree water variability, *J. Mar. Res., 40,* suppl., 757-775, 1982.

Tourre, Y. M., Y. Kushnir, and W.i B. White, Evolution of interdecadal variability in sea level pressure, sea surface temperature, and upper ocean temperature over the Pacific Ocean, *J. Phys. Oceanogr., 29,* 1528-1541, 1999.

Weaver, A. J., and E. S. Sarachik, Evidence for decadal variability in an ocean circulation model: An advective mechanism, *J. Phys. Oceanogr., 29,* 197-231, 1991.

Worthington, L. V., The 18° water in the Sargasso Sea, *Deep Sea Res. Part I, 5,* 297-305, 1959.

Yasuda, T., and K. Hanawa, Decadal changes in the mode waters in the midlatitude North Pacific, *J. Phys. Oceanogr., 27,* 858-870, 1997.

Zhang, R. H., and S. Levitus, Structure and cycle of decadal variability of upper-ocean temperature in the North Pacific, *J. Clim., 10,* 710-727, 1997.

S.S. Drijfhout and W. Hazeleger, Royal Netherlands Meteorological Institute, Oceanography Department P.O. Box 201, 3730 AE De Bilt, The Netherlands. (drijfhou@knmi.nl; hazelege@knmi.nl)

(Received November 23, 1998; revised February 10, 2000; accepted February 10, 2000.)